GPS and CSS Sources — Theory and Modelling

Geoffrey V. Bicknell[1,2], Curtis J. Saxton[1,2] and Ralph S. Sutherland[1]

[1] Research School of Astronomy and Astrophysics, Australian National University, Mt Stromlo Observatory,
Cotter Road, Weston, ACT 2611, Australia
geoff@mso.anu.edu.au
[2] Department of Physics and Theoretical Physics, Australian National University,
Canberra, ACT 0200, Australia

Abstract: We review theoretical ideas that seem to be currently important for the physics of GPS and CSS radio sources. These include models for their evolution, the production of emission lines, and the origin of the low frequency turnover. We also describe the initial phases of a program of simulations that is aimed at understanding the radiative interactions between jets, lobes, and dense clouds in the nuclei of these objects.

1 Introduction

The study of GPS and CSS sources is one which is rapidly evolving both with observational advances and theoretical ideas to explain this important section of the radio luminosity function. There seems little doubt that in most cases we are studying young radio galaxies — in some cases very young — and that these objects represent the very early stages of mature objects such as Cygnus A and 3C 31 that have been the focus of much radio galaxy research to date. Our study of GPS and CSS sources should eventually yield some important clues as to what actually forms a radio galaxy and the subject is quite obviously poised at a very interesting stage.

At Mt Stromlo, we have been mainly focused on the relationship between the radio and optical properties of GPS and CSS sources and principally on the production of emission lines. However, as we shall see, the physical models that we construct have important implications for the environment of the radio source, the structure of the interstellar medium, the radio rotation measure, and the way in which the sources evolve. In this paper we touch on all of these topics and present the first simulations of jets interacting with a clumpy interstellar medium.

2 Evolution of GPS and CSS Sources

A good place to begin when discussing GPS and CSS sources is the relationship between size and age since this involves both the power of the jet driving the expansion of the radio lobe and the properties of the ambient medium. In his initial models for compact symmetric objects, Begelman (1996) conjectured that the evolution of a lobe would occur in such a way that the mean hot-spot pressure would be approximately a constant factor (here denoted by ζ) times the cocoon pressure. He justified this by examining the initial stages of simulations by Lind et al. (1989) concluding that $\zeta \approx 2$; the conjecture has since been verified in detail for the propagation of over-pressured lobes (Carvalho & O'Dea 2002a, 2002b; see

also O'Dea these proceedings). Bicknell, Dopita, & O'Dea (1997, hereafter BDO) refined the Begelman (1996) model by allowing for expansion losses. In terms of parameters relevant for CSS sources, the velocity of advance of the bow shock into a smooth ambient medium whose density varies with distance R from the core as $R^{-\delta}$ with hydrogen number density n_0 at a fiducial radius of 1 kpc and jet energy flux F_E is given by

$$\left(\frac{v_b}{c}\right) \approx 0.056 \left[\frac{F_{E,46}}{n_0(\text{kpc})/0.01\text{cm}^{-3}}\right]^{1/3} \left[\frac{R}{\text{kpc}}\right]^{(\delta-2)/3}. \tag{1}$$

In order to reproduce the number–size relation Begelman (1996) adopted $\delta \approx 1.5$, consistent with the slope of X-ray atmospheres. In the above expression, the fiducial value of $n_0(\text{kpc}) = 0.01$ cm^{-3} is typical of the atmospheres of giant ellipticals.

In order to model the emission line luminosity from regions shocked by the advancing bow shock, BDO used a lower jet power and a larger number density in order to be consistent with the observed line widths $\sim$500–1000 km s^{-1}. However, recent measurements of advance speeds $\sim$0.1 c (see the review by Conway 2002; Murgia et al. 1999; Murgia 2003) are consistent with the fiducial values of the parameters given in equation (1). If line-emitting clouds are to be ionised by the advancing bow shock then the medium must be clumpy, possibly with a fairly low filling factor so that the advance of the lobe is not substantially impeded. An additional argument in favour of $F_E \sim 10^{46}$ erg s^{-1} is that the ratio of 5 GHz radio power to jet energy flux,

$$\kappa_5 = \frac{P_5\,\text{GHz}}{F_E} \approx 10^{-11.5} \left(\frac{P/10^{27.5}\,\text{W Hz}^{-1}}{F_E/10^{46}\,\text{erg s}^{-1}}\right)\,\text{Hz}^{-1}, \tag{2}$$

lies within a more conventional range than that adopted by BDO.

Putting equation (1) into a form more relevant to GPS parameters, we have, for $\delta = 1.5$,

$$\left(\frac{v_b}{c}\right) \approx 0.056 \left[\frac{F_{E,46}}{n_0(100\,\text{pc})/0.01\,\text{cm}^{-3}}\right]^{1/3} \left[\frac{R}{100\,\text{pc}}\right]^{-1/6}. \tag{3}$$

This advance velocity is consistent with the measurements by Conway (2002) and his estimate of the density from the momentum balance at the hot spot. The equations for hot-spot advance speed emphasise the minor dependence on radius.

A 'dentist drill' type evolution of the lobe (Scheuer 1982) resulting from jet–cloud encounters could also enforce a self-similar type advance, although this may not be necessary for the reasons mentioned above.

To summarise, the velocities of advance of the lobes of GPS and CSS sources are consistent with a self-similar model involving conventional ISM number densities and conventional ratios of radio power to jet energy flux. Note, however, that we are talking about very powerful (Cygnus A power) radio sources; less powerful sources such as those discussed by Drake et al. (2003) are expected to expand at a much lower speed.

3 Emission Lines and the Absorption Mechanism

As we indicated above the BDO model was motivated, in part, by the need to explain the emission line fluxes from GPS and CSS sources. It was also thought that the ionised gas surrounding the source could be responsible for the free–free absorption of the radio emission. The features of this model are:

- A radiative bow shock expanding into the interstellar medium at a speed $\sim$200–1000 km s^{-1}.
- Emission lines resulting from the shocked clouds and from clouds in front of the bow shock that are photo-ionised by the radiation from the shocks.
- A turnover in the radio spectrum at low frequencies resulting from free–free absorption by the shock- and photo-ionised gas. BDO explained the relationship between turnover frequency and size using this model. A high ISM density at 1 kpc was required to explain both the slow expansion and the free–free absorption.
- A low frequency power-law slope resulting from a distribution of optical depths.

Some observations support the fundamental tenets of this model. For example, Kameno et al. (2000) have verified that free–free absorption applies in the GPS source OQ 208. de Vries et al. (1997, 1999) have shown radio emission line alignment in CSS galaxies; O'Dea et al. (2002) have discovered systematic velocity offsets of the emission lines of the order of 300–500 km s^{-1} together with broad $\sim$500 km s^{-1} profiles and split lines. The latter three papers are strongly consistent with shock excitation of the gas.

In another clever piece of observational work, Mutoh et al. (2002) inferred that synchrotron self-absorption is

not the preferred absorption mechanism in a GPS sample by demonstrating the absence of a change of polarisation across the peak of the spectrum. On the other hand, Fanti & Fanti (2002) have offered an appealingly simple model that explains the low frequency turnover in terms of synchrotron self-absorption. For a fixed source luminosity of 10^{27} W Hz^{-1}, they calculate the corresponding minimum energy magnetic field as a function of size and from that calculate the frequency at which the spectrum would turn over because of synchrotron self-absorption. This replicates the anti-correlation between turnover frequency and size quite nicely (see Figure 1) and represents a strong case for synchrotron self-absorption. Whilst we generally like to explain everything with one model, it is possible that both free–free absorption and synchrotron self-absorption dominate in different sources.

It is possible that *both* absorption mechanisms play a role. Given the amount of ionised gas related to GPS and CSS sources, as revealed by the emission line nebulosity, it is feasible that free–free absorption plays a role in the larger CSS sources as well as the smaller GPS ones for which we have cited direct evidence. This refers mainly to sources that are (at least in projection) contained within the optical emission line image.

4 Modification of the Radiative Bow-Shock Model

Returning to the BDO model, it is now apparent that, despite some qualitative agreement with some of the key observational aspects of CSS sources, it has some significant problems. These include:

- In most of the CSS sources imaged by de Vries et al. (1999), the line emission is not concentrated at the head of the radio lobe; it trails the radio emission significantly. An example is shown in Figure 2.
- CSS expansion speeds are of order $(0.01$–$0.07)\,c$.
- GPS expansion speeds are of order $(0.1$–$0.3)\,c$.
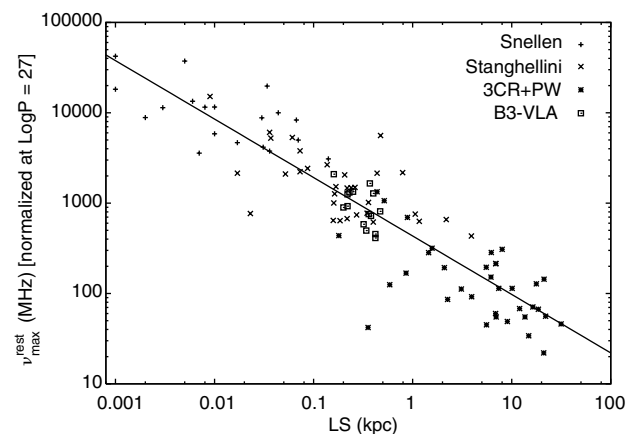- The model predicts very large rotation measures.

Figure 1 The solid line represents the theoretical relation between turnover frequency and linear size derived by Fanti & Fanti (2002) on the basis of their synchrotron self-absorption model. The data points were obtained from the literature.

These facts motivated de Vries et al. (1999) to consider a partial modification of the BDO model and in Section 4.2, below, we present a further revision of that model. Before doing so however, let us discuss some of the properties of radiative shocks that are relevant to a discussion of shock-excited emission lines in GPS and CSS sources.

4.1 The Formation of an Optically Radiating Shock

In the theory to follow, the time taken for a shock to become fully radiative is important in determining the distribution of optical line emitting gas around the advancing lobe. Figure 3 shows profiles of number density and temperature as a function of the parameter nt, where n is the pre-shock hydrogen density and t is the time, relative to when a parcel of gas passes through the shock.
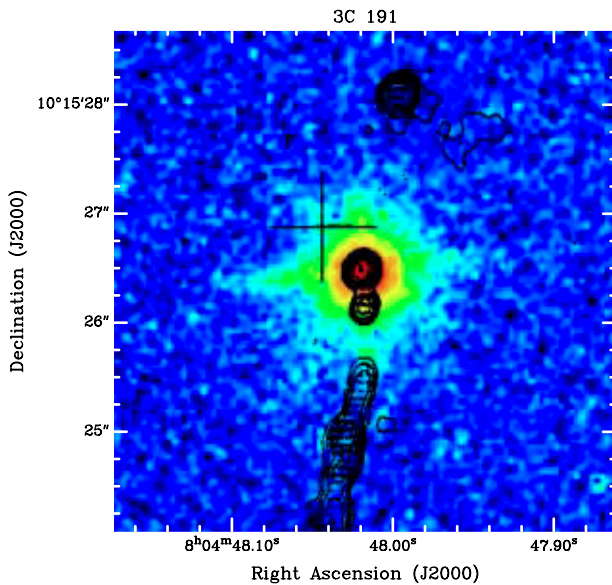

Figure 2   Radio–optical image of the CSS source 3C 191 (de Vries et al. 1997). The radio source is seen to be more extended than the emission line gas which is distributed on a scale $\sim$kpc.

(See Dopita & Sutherland (2002) for a more complete description of the physics of this plot.) Note that, in this case, the temperature of the gas drops to about 10^4 K when $nt \approx 2.2 \times 10^{12}$ cm^{-3} s.

The time, t_4, for a shock to become fully radiative is conveniently defined by the point at which the temperature drops precipitously from values $\sim 10^6$ K in the hot/cooling zone to $\sim 10^4$ K in the photoionised zone. This parameter is a function of shock velocity as shown in Figure 4 and can be conveniently represented by the approximate fitting function:

$$t_4 \approx 2.3 \times 10^4 \, n^{-1} \left(\frac{v_{\rm sh}}{300 \, {\rm km \, s^{-1}}} \right)^{3.9} \, {\rm yr}. \qquad (4)$$

(See Sutherland (1993) and Dopita & Sutherland (1995, 1996) for the description of the MAPPINGS code and calculations that are the basis of this plot.)
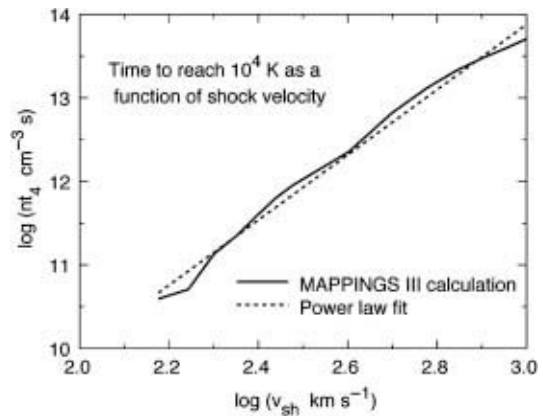

Figure 4   Plot of the parameter pre-shock hydrogen density × time taken to reach optically emitting temperatures (nt_4) versus shock velocity. The results of detailed calculations with the MAPPINGS III code (see Sutherland & Dopita 1993; Dopita & Sutherland 1995, 1996) are shown by the solid line. The approximate fitting function described in the present text is shown by a dashed line.
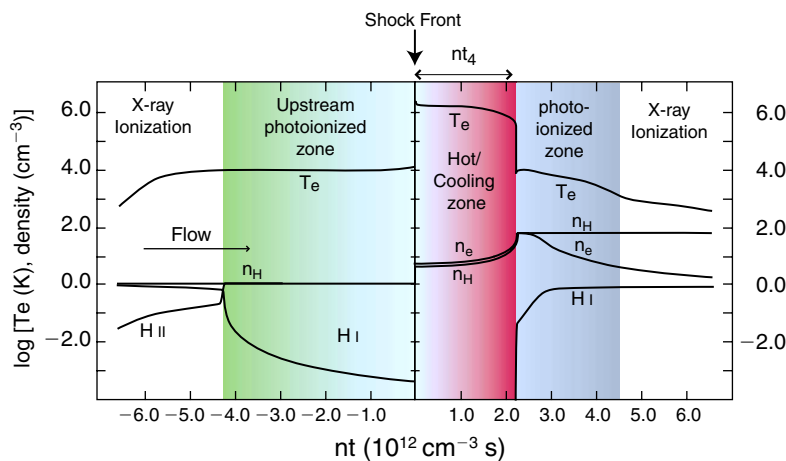

Figure 3   Profiles of density and temperature in a radiative shock with a velocity of $400 \, {\rm km \, s^{-1}}$. The curves show the temperature, density and ionisation fraction history of a parcel of gas that passes through the shock at $t = 0$ as a function of the parameter pre-shock hydrogen density × time (nt). The parameter nt is used since the cooling time is inversely proportional to density.

By way of example, a shock with a velocity of $500\,\mathrm{km\,s^{-1}}$ in a cloud of density $10\,\mathrm{cm^{-3}}$ takes 2.1×10^4 yr to become fully radiative. In this time a $0.1\,c$ bow shock travels 650 pc. Thus the radio source can expand by a considerable amount before a cloud shock becomes fully radiative. This comparison can be be quite an important constraint on the relative locations of radio and optical emission.

4.2 Shocking of a Clumpy Medium by an Expanding Radio Source

de Vries et al. (1999) realised that the finite cooling time of shocked gas could be responsible for the trailing of the optical emission in CSS sources. On the other hand, radio–optical morphologies represented by 3C 191 (Figure 2) could simply be the result of the radio source breaking out of a dense, cloudy environment in the environs of the galactic nucleus. This has been the approach adopted by Dopita (2002) in constraining the regions of AGN that are shock-excited or photoionised. Nevertheless, the physics identified by de Vries et al. (1999) is important for determining the conditions for the production of line emission from an advancing lobe. We therefore summarise the de Vries et al. (1999) analysis here, with the additional modification implied by the above considerations of radiative shocks.

Figure 5 schematically shows clouds that have been swept up by the advancing bow shock. Inside the bow shock the pressure, p_b, is determined from the bow-shock advance velocity and is given by

$$p_b \approx \frac{3}{4}\mu n_{\mathrm{ism}} m_p v_b^2$$
$$= 7.0 \times 10^{-6} n_{\mathrm{ism}} \left(\frac{v_b}{0.1\,c}\right)^2 \mathrm{dyn\,cm^{-2}}. \quad (5)$$
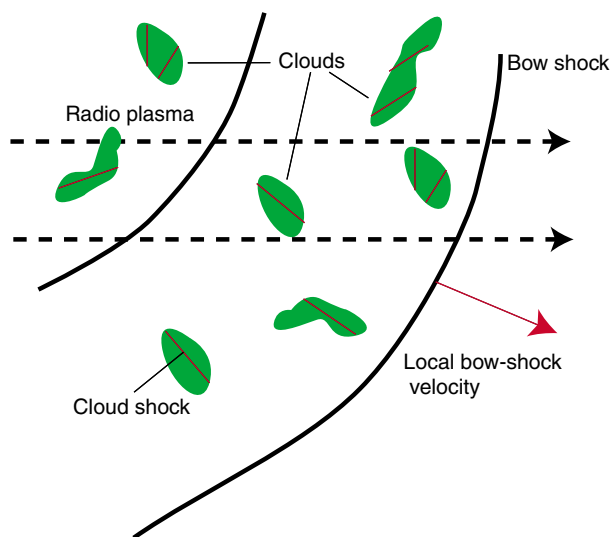

Figure 5 Cartoon of clouds that have been overtaken by an advancing bow shock and some of which have been mixed into the radio plasma. Radiative shocks are driven into the clouds by the excess pressure of the cocoon. The dashed lines illustrate the covering factor of the shocks intercepted by one resolution element of the optical image.

The velocities of the cloud shocks are determined from the cloud density, n_{cl}, and the interstellar medium density, n_{ism}, by

$$v_{\mathrm{sh}} \approx v_b \left(\frac{n_{\mathrm{cl}}}{n_{\mathrm{ism}}}\right)^{-1/2}$$
$$\approx 300 \left(\frac{n_{\mathrm{cl}}/n_{\mathrm{ism}}}{10^4}\right)^{-1/2} \left(\frac{v_b}{0.1c}\right) \mathrm{km\,s^{-1}}. \quad (6)$$

It is reassuring that shock velocities of the right order of magnitude are produced in clouds with a density contrast $\sim 10^4$ with the background medium. This is the sort of density contrast that one expects of clouds with temperature $T_{\mathrm{rmcl}} \sim 10^3\,\mathrm{K}$ immersed in an ISM with $T_{\mathrm{ism}} \sim 10^7\,\mathrm{K}$. The time for such a shock to become fully radiative is given by

$$t_4 \approx 2.3 \times 10^4 \, n_{\mathrm{cl}}^{-1} \left(\frac{v_{\mathrm{sh}}}{300\,\mathrm{km\,s^{-1}}}\right)^{3.9} \mathrm{yr}. \quad (7)$$

In order to ascertain whether a given lobe, of radial extent R, will exhibit optical emission, we need to compare this with the dynamical time,

$$t_{\mathrm{dyn}} \approx \frac{R}{v_b} \approx 1.6 \times 10^5 \left(\frac{R}{\mathrm{kpc}}\right) \left(\frac{v_b}{0.1\,c}\right)^{-1} \mathrm{yr}. \quad (8)$$

The condition for an optical display from the radiative shock is

$$t_4 < f\,t_{\mathrm{dyn}} \qquad f \sim 1 \quad (9)$$

implying that

$$\left(\frac{v_b}{c}\right) < 0.024 \, f^{0.2} \, n_{\mathrm{cl}}^{0.2} \left(\frac{n_{\mathrm{cl}}/n_{\mathrm{ism}}}{10^4}\right)^{0.4} \left(\frac{R}{5\,\mathrm{kpc}}\right)^{0.2}. \quad (10)$$

An appealing feature of this expression is that the estimate of the upper limit on the bow-shock velocity is fairly insensitive to density parameters and the precise value of f. Note that v_b is the *local* bow-shock velocity and not simply the velocity of the apex of the bow shock. Because of the dependence of v_b on location on the bow shock, the inequality may not be satisfied at the apex of the bow shock but may be satisfied on the sides providing a possible explanation for the trailing line emission noted above. At the same time we emphasise the alternative that in sources like 3C 191, the radio source may be breaking free of the nuclear environment and that the line emission simply traces the location of the dense gas. We discuss this further below. Nevertheless, the expression gives useful limits on the relevant bow-shock velocities. For example, for $n_{\mathrm{cl}} \sim 100\,\mathrm{cm^{-3}}$ and $n_{\mathrm{cl}}/n_{\mathrm{ism}} \sim 10^4$, the critical bow-shock velocity is approximately $0.06\,c$. This is within the range of observed velocities.

4.3 A Case Study: 3C 303.1

Let us consider the application of some of these ideas to 3C 303.1 shown in Figure 6. The estimated expansion speed of this source is $0.07\,c$ (O'Dea et al. 2002) compatible with the limit on the bow-shock velocity derived above.
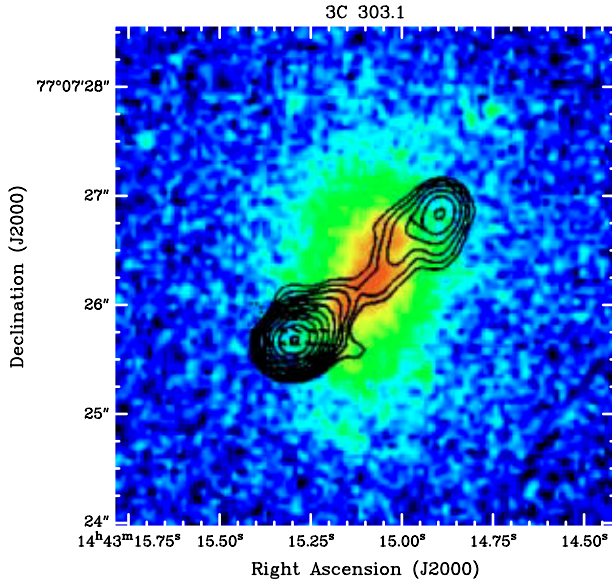
Figure 6 Radio–optical image of 3C 303.1 provided by W. de Vries.

The surface brightness of the [O III] emission together with emission line velocities for this source and others is given in de Vries et al. (1997, 1999). In the following, we constrain the number density and covering factor that are implied by the observations of this source.

Consider a shock of velocity $1000\,v_{\mathrm{sh},3}$ km s^{-1} progressing into a dense cloud whose hydrogen density is n_H cm^{-3}. The luminosity per unit area of the shock in [O III] $\lambda\,5007 \approx 2.3 \times 10^{-2}\,n_H v_{\mathrm{sh},3}^3$ for a matter-bounded cloud (BDO). Therefore for an unresolved clumpy medium, the surface brightness of [O III] is given by

$$I(\text{[O III]}) \approx 2.3 \times 10^{-2} \times CF \times n_H v_{\mathrm{sh},3}^3, \quad (11)$$

where we define the covering factor, CF, to be the fraction of shock area within a given observed area along the line of sight. Note that this expression assumes that the shock precursor in the cloud is optically thick (i.e. matter bounded). If this is not the case then the above expression represents an upper limit to the surface brightness.

Consistent with the observations, let us assume a shock velocity ≈ 400 km s^{-1}. Comparing the surface brightness with the peak observed surface brightness in [O III] implies $CF \times n_H > 47$ cm^{-3}. We have an independent estimate for n_H from the shock velocity. Using equation (6) we obtain

$$n_{\mathrm{cl}} \approx 6 \left(\frac{n_{\mathrm{ism}}}{10^{-2}\,\text{cm}^{-3}} \right) \text{cm}^{-3}. \quad (12)$$

Hence, in this case, the covering factor, $CF > 33$, i.e., the emission line region surrounding the radio source is quite substantial.

We can now assess whether the shocked clouds are likely to be matter bounded, i.e. are all of the ionising photons emitted by a given cloud shock likely to be absorbed by the precursor gas? To answer this we consider the column density, n_c, of the Strömgren zone which is given by

the following fitting formula (Dopita & Sutherland 1996) in which V_{100} is the shock velocity in units of 100 km s^{-1}:

$$\log \left(\frac{n_c(\text{H II})}{\text{cm}^{-3}} \right) = 19.50 + 2.933 \log V_{100}$$
$$+ 0.029 \log^2 V_{100}. \quad (13)$$

Taking the width of the Strömgren zone, L_{st}, to be given by $n_H L_{\mathrm{st}} \approx n_c$, then L_{st} for a 400 km s^{-1}, 6 cm^{-3} shock is about 44 pc. The resolution of the HST optical image is approximately 660 pc so that clouds of the Strömgren size would be unresolved.

The Jeans length is another constraint to take into account. For a sound speed, c_s, and density $\rho_{\mathrm{cl}} = 1.4\,n_H m_p$, the Jeans length is

$$\lambda_J = 2\pi \sqrt{c_s^2 4\pi G \rho_{\mathrm{cl}}} \approx 1.7\,T_4^{1/2} n_H^{-1/2} \text{ kpc}. \quad (14)$$

For $n_H = 6$ cm^{-3} the Jeans length ≈ 460 pc $\approx 0.10''$. This length comfortably exceeds the width of the Strömgren zone, so that Jeans-stable matter-bounded clouds with the inferred density can exist.

The Roche radius for tidal disruption of clouds by the central black hole should also be considered. The Roche radius for tidal disruption of a spherical cloud of mass M_{sl}, radius R_{cl}, and density ρ_{cl} by a black hole of mass M_H is

$$R_R = \left(\frac{M_H}{M_{\mathrm{cl}}} \right) R_{\mathrm{cl}} = \left(\frac{3}{4\pi} \right)^{1/3} \left(\frac{M_H}{\rho_{\mathrm{cl}}} \right)^{1/3}$$
$$\approx 0.89 \left(\frac{M_H/10^8 M_\odot}{n_H} \right)^{1/3} \text{ kpc}. \quad (15)$$

The Roche radius is interesting, perhaps not so much for 3C 303.1 where it would be unresolved, but for GPS sources. Clouds with $n_H = 100$ cm^{-3} would be tidally disrupted within 400 pc of a $10^9\,M_\odot$ black hole. This should be taken into account in future application of these ideas to GPS sources. Note that black holes of at least 10^8–$10^9\,M_\odot$ are indicated since the corresponding Eddington luminosity $L_{\mathrm{edd}} = 10^{46}$–$10^{47}$ erg s^{-1}.

In the present context of 3C 303.1, however, there appear to be no physical reasons against the existence of matter-bounded clouds with densities ~ 6 cm^{-3}, sizes ~ 60 pc, and a covering factor ~ 0.04. On the other hand the clouds could be smaller, ionisation bounded, and correspondingly denser with a larger covering factor. Further consideration of the rotation measure and free–free absorption properties in the context of models for the emitting region are necessary.

Nevertheless, we can examine whether free–free absorption is likely to be important in 3C 303.1. Using the expression for the optical depth to free–free absorption from the shocked region of a matter-bounded cloud (BDO), the *mean* free–free optical depth from the ensemble of clouds within a beam is

$$\langle \tau_\nu \rangle \approx CF \times n_H \times \left(0.38 V_{100}^{2.3} + 0.03\,V_{100}^{1.5} \right) \nu_9^{-2.1}, \quad (16)$$

where ν_9 is the frequency in GHz and the first and second terms represent the contribution from the shocked and photoionised regions respectively. Note that this optical depth is an average. There will be lines of sight with larger and smaller optical depths; the statistical distribution depends upon the density of the intercloud medium. As we show in the next section, this can be substantially affected by the passage of the shock. Using this expression and the inferred value of $CF \times n_H$ predicts a turnover frequency $\nu_t \approx 164\,\text{MHz}$ compared with an observed turnover at approximately $50\,\text{MHz}$. Note that the turnover is relatively insensitive to the precise value of the density since $\nu_t \propto (CF \times n_H)^{0.48}$.

This turnover frequency only applies to that part of the source that we know to be partially covered by ionised gas, i.e., the emission line region. If free–free absorption is important for the part of the radio source near the apex of the radio lobe, then invisible ionised clouds are required. As indicated in the discussion in Section 4 it is possible that there are shocked (mainly X-ray emitting) clouds in this region that are not strongly emitting optically and these would contribute a similar optical depth. The presence of such clouds would be apparent in rotation measure images. Thus rotation measure imaging emerges as a diagnostic tool for investigating the environment of these sources (see Cotton et al. 2003).

5 Simulations of Radio Source Cloud Interactions

Given the questions raised by the above physical discussion, there is strong motivation for a program of simulations, to study in detail the nature of radio source–ISM interactions in an inhomogeneous medium. In such simulations the physics of radiative shocks needs to be captured adequately; good resolution is required in order to understand the physics of non-thermal plasma–cloud interactions and the effect on the radio source of the inhomogeneities in the interstellar medium.

We have been developing the numerical code to study these interactions using as a basis the VH-1 code developed by a group of numerical astrophysicists originally based at the University of Virginia.[1] This initially adiabatic PPM code (Colella & Woodward 1984a, 1984b) has been enhanced for computational efficiency and the dynamical effects of radiative cooling have been included. We found when modelling radiative shocks with this code that they developed a 'striping' numerical instability that was exacerbated by cooling. An 'oscillation filter' method for dealing with this instability has been successfully implemented (Sutherland, Bisset, & Bicknell 2002). The code has recently been ported to the MPI parallel environment; however, the results presented here have been obtained from the single processor version. With this version, three-dimensional jet simulations would be too costly. Therefore, in order to obtain an idea of the effect of the cloud distribution on radio source dynamics, and to
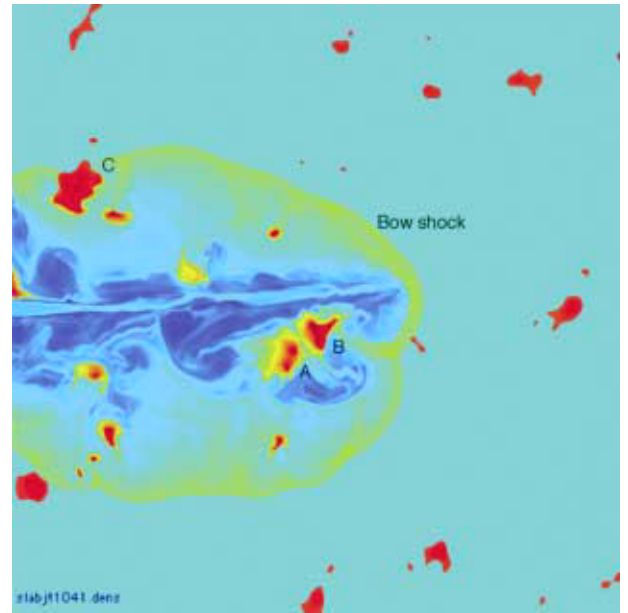

Figure 7 Logarithmic density snapshot from a simulation showing the interaction of a jet with a medium of low filling factor. The lowest density gas (jet and cocoon) is dark blue, the intermediate density gas (the ISM) is cyan, and the dense clouds are red. The shocked ISM appears as yellow. Radiative shocks being driven into the dense clouds appear almost black.

map out interesting regions of parameter space, we are in the process of conducting a series of slab jet simulations.

Rather than simply lay down a set of spherical clouds, on either a random or ordered grid, we have adopted the following procedure for generating a hot interstellar medium with embedded dense clouds. An inhomogeneous medium is generated in Fourier space by initially assigning random phases to each point of a grid. The Fourier spectrum is then multiplied by a power law in wavenumber with lower and upper cutoffs defined by the Jeans scale and the grid resolution respectively. The Fourier transform is inverted and scaled to give arbitrarily shaped regions of fluctuating density. Truncation of the density below a preassigned level and filling of the regions in between by pressure matched hot gas gives a distribution of dense clouds in a hot medium. Variation of the truncation level affects the filling factor of the dense clouds.

Figure 7 shows a logarithmic density snapshot from a simulation in which a slab jet passes through a medium of clouds constructed in this fashion. A movie of this simulation (slab_02) is available.[2] The jet is initially deflected by the cloud that is located near the inlet. It then hits the two large clouds (A and B) near the jet terminus and the resultant reverse shock deflects the jet upwards. In the colour version of this picture one can readily recognise radiative shocks (the dark regions) being driven into these clouds as a result of the jet impact. The large cloud (C) near the top left hand edge of the cocoon also reveals

[1] http://wonka.physics.ncsu.edu/pub/VH-1/

[2] http://macnab.anu.edu.au/radiojets/gps/

a radiative shock that is driven into it solely by the pressure of the shocked gas inside the bow shock. The bow shock is revealed by the yellow region enveloping the blue non-thermal gas.

Figure 8 shows a logarithmic density snapshot from a different simulation in which the filling factor of the clouds is much greater. This simulation is an excellent illustration of what would happen to a jet that is frustrated by its environment. Again, a movie of this simulation (and others) can be obtained from the latter web address.

In this case, the jet breaks into a few different channels as a result of its interaction with impeding clouds. The result is an expanding energy driven bubble that may be affected by the cooling gas being ablated from the clouds.

There is another feature of these simulations that is more apparent in the movies, and that is the clouds in the first simulation are inclined to spread sideways more than in the second simulation. The difference is related to the degree to which the shocks are radiative. When a cloud shock is adiabatic, the acceleration of the cloud makes it 'pancake' (i.e. become thinner in the stream direction);
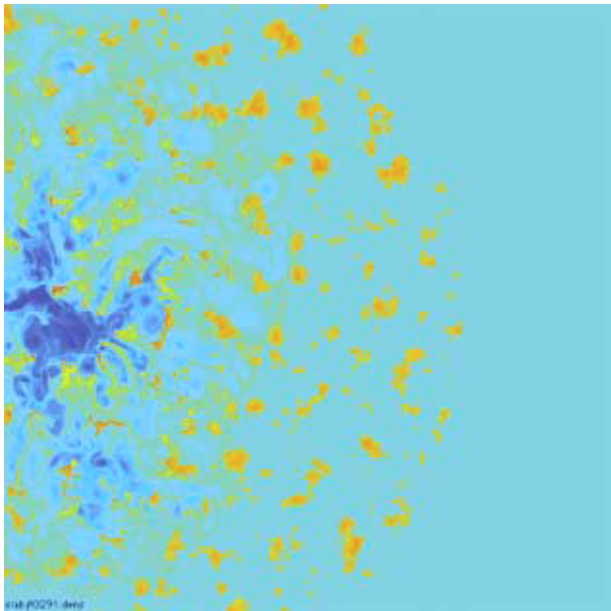

Figure 8 Logarithmic density snapshot from a simulation showing the interaction of a jet with a medium of high filling factor. The colour scheme is similar to the previous snapshot, except that in this case the dense clouds appear orange. The radiative shocks are a darker shade of orange. Note the breaking up of the jet into a number of separate channels.

this is a result of the cloud adjusting to the local gravitational field in its own rest frame. When the shock is highly radiative, the large compression of the cloud by the shock counteracts this effect and the cloud stays more or less the same size. In the second simulation the shocks are more strongly radiative, hence the smaller lateral spread. One of the consequences of this interaction is that the clouds obstruct the flow (specifically the jet) for longer than the nominal 'few shock crossing times' that are usually invoked in such situations.

The parameters of the above simulation are summarised in Table 1. Most of the parameters are obvious. The parameters $\eta = \rho_{jet}/\rho_{ism}$ and $\xi = p_{jet}/p_{ism}$ are the initial ratios of jet to ambient density and pressure respectively. The parameter M_{jet} is the jet Mach number; R_{jet} is the half thickness of the jet (i.e. it is equivalent to the radius of a three-dimensional jet; β_{bs} is an estimate of the bow-shock velocity using $\eta^{1/2}\beta_{jet}$; F_E is the energy flux of the three dimensional jet with the parameters of the previous columns and a radius of R_{jet}. The cloud parameters are the minimum ($n_{cl,min}$) and mean ($\bar{n}_{cl}$) cloud densities relative to the external medium, and the filling factor of clouds (f_{cl}). Note that the velocities implied are relativistic ($0.6\,c$ in one case) and that we are using a non-relativistic code. In the initial analysis, it is mainly the energy and momentum transported by the jet that are important. However, in future, we shall have to consider the implementation of a relativistic PPM code. Further simulations with different parameters have also been carried out and are obtainable at the above web address.

There are strong similarities between clouds shocked by the pressure of the bow shock and clouds in the ISM shocked by the passage of a supernova blast wave, e.g. cloud C in Figure 7. The main difference for clouds shocked in this way is in the speed of the shocks, with most supernova-induced shocks being of low velocity (i.e. less than $150\,\mathrm{km\,s^{-1}}$). However, there is an additional feature here and that is the direct jet–cloud encounters that have no counterpart in the environment of supernova blast waves.

Our program of simulations is continuing with attention soon to be given to three dimensional simulations that are selected on the basis of the parameter space mapped out by the two dimensional work. This has been made possible by the revision of our code to an MPI version by S. Midgley from the ANU Supercomputer Facility. The new code will be capable of using the full 500 processors of the Compaq supercomputer installed at ANU by the Australian Partnership for Advanced Computation (APAC).

Table 1. The parameters of the slab jets discussed in this paper

Model	η	ξ	n_{ism} (cm^{-3})	T_{ism} (K)	M_{jet}	R_{jet} (pc)	β_{jet}	β_{bs}	F_E (erg s^{-1})	$n_{cl,min}/n_{ism}$	n_{cl}/n_{ism}	f_{cl}
slab 02	0.38	130	0.01	10^7	35	25	1.0	0.62	10^{45}	300	480	0.029
slab 09	0.0011	1.0	1.00	10^7	130	10	6.0	0.2	10^{46}	500	1000	0.117

Acknowledgments

References

Begelman, M. C. 1996, in Cygnus A: Study of a Radio Galaxy, eds C. L. Carilli & D. A. Harris (Cambridge: Cambridge University Press), 209

Bicknell, G. V., Dopita, M. A., & O'Dea, C. P. 1997, ApJ, 485, 112 (BDO)

Carvalho, J. C. & O'Dea, C. P. 2002a, ApJS, 141, 371

Carvalho, J. C. & O'Dea, C. P. 2002b, ApJS, 141, 337

Colella, P. & Woodward, P. R. 1984a, JCoPh, 54, 115

Colella, P. & Woodward, P. R. 1984b, JCoPh, 54, 174

Conway, J. E. 2002, NewAR, 46, 263

de Vries, W. H., O'Dea, C. P., Baum, S. A., & Barthel, P. D. 1999, ApJ, 526, 27

Cotton, W. D., et al. 2003, PASA, 20, 12

de Vries, W. H., et al. 1997, ApJS, 110, 191

Dopita, M.A. 2002, in Emission Lines from Jet Flows, Revista Mexicana de Astronomia y Astrofisica Conference Series Volume 13, ed. W. J. Henney, W. Steffen, A. C. Raga, & L. Binette, 177

Dopita, M. A. & Sutherland, R. S. 1995, ApJ, 455, 468

Dopita, M. A. & Sutherland, R. S. 1996, ApJS, 102, 161

Dopita, M. A. & Sutherland, R. S. 2002, Astrophyics of the Diffuse Universe (Heidelberg: Springer-Verlag)

Drake, C. L., McGregor, P. J., Bicknell, G. V., & Dopita, M. A. 2003, PASA, 20, 57

Fanti, C. & Fanti, R. 2002, in Issues in Unification of Active Galactic Nuclei, ASP Conference Series 258, ed. R. Maiolino, A. Marconi, & N. Nagar (San Francisco: ASP), 261

Kameno, S., Horiuchi, S., Shen, Z., Inoue, M., Kobayashi, H., Hirabayashi, H., & Murata, Y. 2000, PASJ, 52, 209

Lind, K. R., Payne, D. G., Meier, D. L., & Blandford, R. D. 1989, ApJ, 344, 89

Murgia, M. 2003, PASA, 20, 19

Murgia, M., Fanti, C., Fanti, R., Gregorini, L., Klein, U., Mack, K.-H., & Vigotti, M. 1999, ApJ, 290, 86

Mutoh, M., Inoue, M., Kameno, S., Asada, K., Kenta, F., & Uchida, Y. 2002, PASJ, 54, 131

O'Dea, C. P., et al. 2002, AJ, 123, 2333

Scheuer, P. A. G. 1982, in Extragalactic Radio Sources, IAU Symposium 97, ed. D. S. Heeschen & C. M. Wade (Dordrecht: Reidel), 163

Sutherland, R. S. 1993, PhD thesis, Mt Stromlo and Siding Spring Observatories, Australian National University

Sutherland, R. S., Bisset, D. K., & Bicknell, G. V. 2003, ApJS, submitted